applied optics

Analysis and correction of misalignment-induced aberrations in two-mirror telescopes with stop on the secondary mirror

Yang Wang,[1] Yingrui Li,[1] Zhiyuan Gu,[2,*] Lei Zhang,[1] and Yuegang Fu[1]

[1]School of Opto-Electronic Engineering, Changchun University of Science and Technology, Changchun, 130022, China
[2]Changchun Institute of Optics, Fine Mechanics and Physics, Chinese Academy of Sciences, Changchun, 130033, China
*Corresponding author: zhiyuan.gu@hotmail.com

Received 14 October 2022; revised 13 December 2022; accepted 31 December 2022; posted 3 January 2023; published 2 February 2023

We study the problem of misalignment aberration analysis and correction of the two-mirror telescopes with stop on the secondary mirror. The variation law of the system's aberration field is analyzed with nodal aberration theory when the primary mirror with an astigmatic figure error is misaligned. The analytic expression among the system wave aberration, misalignments, and astigmatism figure error is given, and the correction model of system misalignment aberration is established. The simulation experiment shows that the relative error of the prediction of system misalignment coma and astigmatism based on this model is less than 4.1%.

https://doi.org/10.1364/AO.478248

1. INTRODUCTION

The two-mirror telescope has a wide range of applications in the field of astronomical observation due to its simple structure, chromatic aberration-free, and large aperture. After the optical design, the processing quality of the mirrors and the alignment have an important influence on the imaging quality of the telescope. Therefore, the analysis and correction of the misalignment aberration of the two-mirror telescopes are meaningful.

The influence of the misalignment on the aberration field in the two-mirror telescope was studied by Schmid [1] with the nodal aberration theory (NAT); the influence of astigmatism and the figure error of the primary mirror (PM) on the aberration field in the R-C telescope was also analyzed [2,3]. The research points out that the astigmatic error of the PM and the misalignment of the secondary mirror (SM) would change the system's astigmatic field, resulting in the phenomenon of "binodal astigmatism." The midpoint of the two astigmatic nodes introduced by the astigmatic figure error of the PM (at the pupil) was located at the center of the field of view (FOV), while one of the two astigmatic nodes introduced by the SM misalignment (in a coma-compensated state) was located at the center of the FOV, and another was in the off-axis FOV. Schmid also pointed out that, when there was no figure error in the two-mirror telescope and the misalignment coma was corrected, there was still residual misalignment astigmatism, and one of the astigmatism nodes was located in the center of the FOV. If there was astigmatism at the central FOV point, this astigmatism was caused by the astigmatic figure error of the optical element (the stop).

On this basis, Gu established a model for calculating the astigmatic error of the PM and the misalignment of the SM in the two-mirror system [4]; further, it was shown that binodal astigmatism and field-constant coma were introduced in the misaligned two-mirror system. Ju considered the calculation of the SM's trilobal error [5]. The trefoil deformation was quantitatively represented in his equation, where it was shown that three additional field-dependent aberration terms were generated in addition to the field-constant elliptical coma (trefoil) term. The methods of Gu and Ju are both analytical based on NAT. In addition, there are numerical methods that can also solve the figure error and misalignment, such as the sensitivity matrix method [6,7] and the optimization function method [8,9]. The numerical misalignment solution method is based on data reduction and numerical methods but without a tie to aberration theory; it is also difficult to reveal the profound internal law among misalignments, figure error, and aberration fields. Therefore, the analytic form of NAT has a natural advantage in analyzing and solving such problems. The aperture stops are set on the PM in most two-mirror telescopes; however, there are also some two-mirror telescopes, such as the large binocular telescope [10], in which the aperture stop is placed on the SM as an adaptive correction element. The research on the misalignment aberration analysis and misalignment calculation of the two-mirror telescopes with the aperture stop on the SM is also meaningful, and this paper analyzes such problems.

The following content of this paper is divided into three parts. The changes of the astigmatic and coma fields of the two-mirror telescopes are analyzed in Section 2, when there are alignment and astigmatic figure errors based on the NAT, and the analytical

forms of misalignments, astigmatic figure error, and wavefront Zernike coefficients are established. Section 3 takes a Cassegrain telescope as an example, wherein the misaligned aberration field is calculated based on the model in this paper and is compared with the ray tracing results. Then, according to the Zernike coefficients of the wavefront, the misalignments and astigmatism figure error of the system are calculated, and the system is corrected by the calculation results. In addition, the correction results are analyzed and discussed. Section 4 concludes this paper.

2. MISALIGNMENT-AFFECTED ABERRATION FIELDS OF TWO-MIRROR TELESCOPES WITH A STOP ON SM

A. Nodal Aberration Theory

The NAT mainly describes the aberration of the optical system when there are misalignment errors in the system. It uses a more general vector form of wave aberration expansion instead of the scalar form in a rotationally symmetric system, which is expressed as

$$W(\vec{H},\vec{\rho}) = \sum_j \sum_{p=0}^{\infty}\sum_{n=0}^{\infty}\sum_{m=0}^{\infty} (W_{klm})_j \left[(\vec{H}-\vec{\sigma}_j)\cdot(\vec{H}-\vec{\sigma}_j)\right]^p \times (\vec{\rho}\cdot\vec{\rho})^n \left[(\vec{H}-\vec{\sigma}_j)\cdot\vec{\rho}\right]^m, \tag{1}$$

where j represents the surface number, W_{klm} is the aberration coefficient, $\vec{H}$ is the FOV vector, and $\vec{\rho}$ is the pupil vector. $\vec{\sigma}_j$ is the introduced field-center displacement vector of surface j; for aspheric surfaces, it is usually decomposed into the spherical base curve and the aspheric departure from the spherical base curve of the surface j. As detailed by Thompson [11,12], the spherical and aspheric component contributions to the aberration field are given by

$$\vec{\sigma}_j^{(\mathrm{sph})} = -\frac{\overrightarrow{\bar{u}^{\#}_{\mathrm{OAR}\,j}} - \begin{bmatrix} -\mathrm{BDE}_j + \mathrm{XDE}_j c_j \\ \mathrm{ADE}_j + \mathrm{YDE}_j c_j \end{bmatrix} + \overrightarrow{\bar{y}^{\#}_{\mathrm{OAR}\,j}}\cdot c_j}{\bar{u}_j + \bar{y}_j c_j}, \tag{2}$$

$$\vec{\sigma}_j^{(\mathrm{asph})} = \frac{1}{\bar{y}_j}\left(\begin{bmatrix} \mathrm{XDE}_j \\ \mathrm{YDE}_j \end{bmatrix} - \overrightarrow{\bar{y}^{\#}_{\mathrm{OAR}\,j}}\right), \tag{3}$$

where $\overrightarrow{\bar{u}^{\#}_{\mathrm{OAR}\,j}}$ and $\overrightarrow{\bar{y}^{\#}_{\mathrm{OAR}\,j}}$ denote the optical axis ray (OAR) paraxial angle and intersection height at surface j referenced to the z axis, respectively; $\bar{u}_j$ and $\bar{y}_j$ correspond to the paraxial chief ray slope angle and height at surface j; and c_j denotes the curvature of surface j. The above definitions are all explained in Fig. 1, and a right-handed coordinate system is utilized in our paper. In a misaligned optical system, there are six types of misalignments, which are the decentering along the x, y, and z axes (XDE, YDE, and ZDE) and the tilt in the $y-z$, $x-z$, and $x-y$ planes (ADE, BDE, and CDE), respectively. A positive XDE/YDE is the displacement in the $+x/y$ direction, and a positive ADE/BDE is left-handed rotation about the $+x/y$ axis.

The wave aberration coefficient W_{klm} has nothing to do with the decentering and tilt of the surfaces, and the pupil correlation of the aberration is also unchanged. Therefore, there is no new type of aberration in the misaligned system, only the field correlation of the aberration has changed.

B. Field-Center Displacement Vectors for Individual Surfaces of Two-Mirror Telescopes with Stop on SM

For studying the misaligned aberration characteristics of the two-mirror telescopes with the stop on the SM, the SM is used as the reference, and the PM is used as the misaligned surface. The PM has six misalignments in total, i.e., $\mathrm{XDE_{PM}}$, $\mathrm{YDE_{PM}}$, $\mathrm{ZDE_{PM}}$, $\mathrm{ADE_{PM}}$, $\mathrm{BDE_{PM}}$, and $\mathrm{CDE_{PM}}$. The $\mathrm{ZDE_{PM}}$ does not destroy the system's symmetry, and it only introduces spherical aberration and defocus, which are easier to correct in the alignment. Because the PM is rotationally symmetric, the $\mathrm{CDE_{PM}}$ does not introduce any aberrations. Therefore, this paper mainly studies four types of misalignments: $\mathrm{XDE_{PM}}$, $\mathrm{YDE_{PM}}$, $\mathrm{ADE_{PM}}$, and $\mathrm{BDE_{PM}}$.

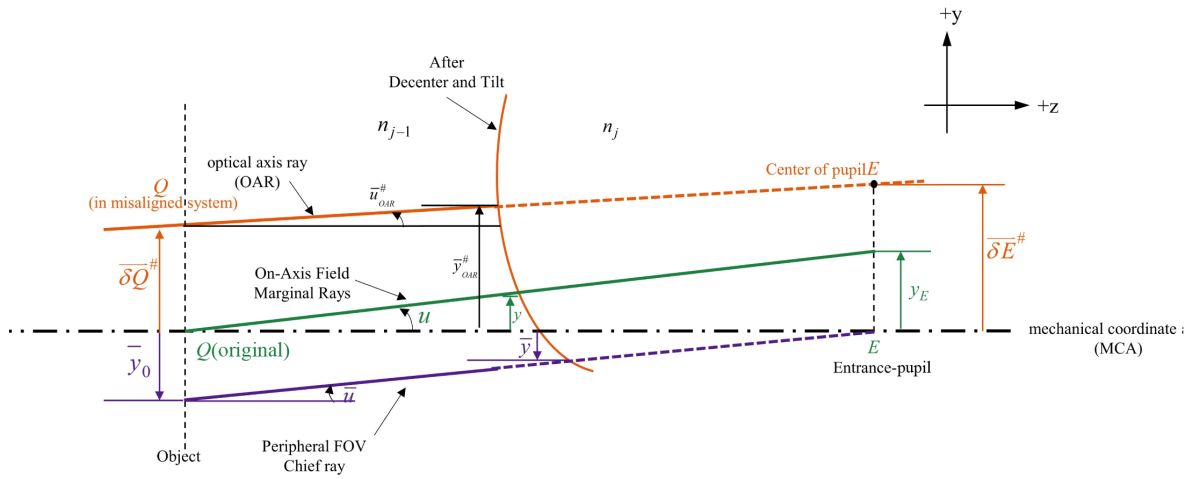

Fig. 1. Definitions of symbols.

Using the paraxial ray tracing equation of the axisymmetric system, we can obtain

$$\bar{u}_{\mathrm{SM}} = \frac{r_{\mathrm{PM}}\bar{u}_{\mathrm{PM}}}{2d_1 - r_{\mathrm{PM}}}, \tag{4}$$

$$\bar{y}_{\mathrm{PM}} = -\frac{d_1\, r_{\mathrm{PM}}\, \bar{u}_{\mathrm{PM}}}{2\, d_1 - r_{\mathrm{PM}}}, \tag{5}$$

$$\bar{y}_{\mathrm{SM}} = 0, \tag{6}$$

where r_{PM} and r_{SM} denote the radius of curvature of the PM and SM, respectively, d_1 denotes the distance from the PM to the SM.

Using the OAR paraxial ray tracing method in the NAT, the paraxial parameters of the OAR in the two-mirror telescopes could be calculated as follows:

$$\overrightarrow{\bar{u}^{\#}_{\mathrm{OAR}\,\mathrm{PM}}} = \begin{bmatrix} 0 \\ 0 \end{bmatrix}, \tag{7}$$

$$\overrightarrow{\bar{u}^{\#}_{\mathrm{OAR}\,\mathrm{SM}}} = -\frac{2}{(2\, d_1 - r_{\mathrm{PM}})} \begin{bmatrix} \mathrm{XDE}_{\mathrm{PM}} - \mathrm{BDE}_{\mathrm{PM}}\, r_{\mathrm{PM}} \\ \mathrm{YDE}_{\mathrm{PM}} + \mathrm{ADE}_{\mathrm{PM}}\, r_{\mathrm{PM}} \end{bmatrix}, \tag{8}$$

$$\overrightarrow{\bar{y}^{\#}_{\mathrm{OAR}\,\mathrm{PM}}} = \frac{2}{(2\, d_1 - r_{\mathrm{PM}})} \begin{bmatrix} \mathrm{XDE}_{\mathrm{PM}}\, d_1 - \mathrm{BDE}_{\mathrm{PM}}\, d_1\, r_{\mathrm{PM}} \\ \mathrm{YDE}_{\mathrm{PM}}\, d_1 + \mathrm{ADE}_{\mathrm{PM}}\, d_1\, r_{\mathrm{PM}} \end{bmatrix}, \tag{9}$$

$$\overrightarrow{\bar{y}^{\#}_{\mathrm{OAR}\,\mathrm{SM}}} = \begin{bmatrix} 0 \\ 0 \end{bmatrix}. \tag{10}$$

Using Eqs. (2) and (3), field-center displacement vectors of the two-mirror telescope with the aperture stop on the SM could be calculated as

$$\vec{\sigma}^{\,(\mathrm{sph})}_{\mathrm{PM}} = -\frac{1}{u_{\mathrm{pr1}}(d_1 - r_{\mathrm{PM}})} \begin{bmatrix} \mathrm{XDE}_{\mathrm{PM}} - \mathrm{BDE}_{\mathrm{PM}} r_{\mathrm{PM}} \\ \mathrm{YDE}_{\mathrm{PM}} + \mathrm{ADE}_{\mathrm{PM}} r_{\mathrm{PM}} \end{bmatrix}, \tag{11}$$

$$\vec{\sigma}^{\,(\mathrm{sph})}_{\mathrm{SM}} = \frac{2}{r_{\mathrm{PM}} u_{\mathrm{pr1}}} \begin{bmatrix} \mathrm{XDE}_{\mathrm{PM}} - \mathrm{BDE}_{\mathrm{PM}} r_{\mathrm{PM}} \\ \mathrm{YDE}_{\mathrm{PM}} + \mathrm{ADE}_{\mathrm{PM}} r_{\mathrm{PM}} \end{bmatrix}, \tag{12}$$

$$\vec{\sigma}^{\,(\mathrm{asph})}_{\mathrm{PM}} = \frac{1}{d_1 u_{\mathrm{pr1}}} \begin{bmatrix} \mathrm{XDE}_{\mathrm{PM}} - 2\mathrm{BDE}_{\mathrm{PM}} d_1 \\ \mathrm{YDE}_{\mathrm{PM}} + 2\mathrm{ADE}_{\mathrm{PM}} d_1 \end{bmatrix}, \tag{13}$$

$$\vec{\sigma}^{\,(\mathrm{asph})}_{\mathrm{SM}} = \begin{bmatrix} 0 \\ 0 \end{bmatrix}. \tag{14}$$

Equations (11–14) give the analytical expression between field-center displacement vectors and the misalignments.

C. Analytical Expression between Zernike Coma Coefficients and Misalignments of Misaligned Two-Mirror Telescopes

According to third-order NAT, in a misaligned system, the coma can be expressed by [11]

$$W_{\mathrm{COMA}_3} = [(W_{131}\vec{H} - \vec{A}_{131}) \cdot \vec{\rho}]\,(\vec{\rho} \cdot \vec{\rho})\,, \tag{15}$$

where $W_{131} = \sum_j W_{131\,j}$ and $\vec{A}_{131} = \sum_j W_{131\,j}\vec{\sigma}_j$.

According to $\vec{\rho} = |\vec{\rho}| \begin{bmatrix} \cos\varphi \\ \sin\varphi \end{bmatrix}$, Eq. (15) could be expressed in matrix form so that it can be decomposed in different directions and combined with Zernike polynomials. The decomposition result is shown in Eq. (16):

$$W_{\mathrm{COMA}_3} = \begin{bmatrix} W_{131}\vec{H}_x - \vec{A}_{131,x} \\ W_{131}\vec{H}_y - \vec{A}_{131,y} \end{bmatrix} \cdot \begin{bmatrix} |\vec{\rho}|^3 \cos\varphi \\ |\vec{\rho}|^3 \sin\varphi \end{bmatrix}, \tag{16}$$

where $\vec{A}_{131x}$ and $\vec{A}_{131y}$ are the x and y components of the $\vec{A}_{131}$, respectively.

According to the relationship between the Seidel coefficients and the Zernike coma coefficients (C_7 and C_8), we can obtain

$$\begin{bmatrix} \vec{A}_{131,x} \\ \vec{A}_{131,y} \end{bmatrix} = \begin{bmatrix} W_{131}\vec{H}_x - 3C_7(\vec{H}) \\ W_{131}\vec{H}_y - 3C_8(\vec{H}) \end{bmatrix}. \tag{17}$$

Therefore, for the case where the stop is on the SM and the PM is misaligned, we can obtain

$$\begin{bmatrix} W_{131}\vec{H}_x - 3C_7(\vec{H}) \\ W_{131}\vec{H}_y - 3C_8(\vec{H}) \end{bmatrix} = \begin{bmatrix} \vec{\sigma}^{\,(\mathrm{sph})}_{\mathrm{PM},x} & \vec{\sigma}^{\,(\mathrm{asph})}_{\mathrm{PM},x} & \vec{\sigma}^{\,(\mathrm{sph})}_{\mathrm{SM},x} \\ \vec{\sigma}^{\,(\mathrm{sph})}_{\mathrm{PM},y} & \vec{\sigma}^{\,(\mathrm{asph})}_{\mathrm{PM},y} & \vec{\sigma}^{\,(\mathrm{sph})}_{\mathrm{SM},y} \end{bmatrix} \begin{bmatrix} W^{\mathrm{sph}}_{131,\mathrm{PM}} \\ W^{\mathrm{asph}}_{131,\mathrm{PM}} \\ W^{\mathrm{sph}}_{131,\mathrm{SM}} \end{bmatrix}. \tag{18}$$

Equation (18) is the analytical expression between the field-center displacement vectors and the Zernike coma coefficients.

D. Analytical Expression between Zernike Astigmatism Coefficients and Misalignments of Misaligned Two-Mirror Telescopes

The third-order astigmatism in the NAT is given by [11]

$$W_{\mathrm{AST}_3} = \frac{1}{2}\left[\sum_j W_{222\,j}\vec{H}^2 - 2\vec{H}A_{222} + \vec{B}^2_{222}\right] \cdot \vec{\rho}^{\,2}, \tag{19}$$

where $W_{222} = \sum_j W_{222\,j}$, $\vec{A}_{222} = \sum_j W_{222\,j}\vec{\sigma}_j$, and $\vec{B}^2_{222} = \sum_j W_{222\,j}\vec{\sigma}^{\,2}_j$.

According to $\vec{\rho}^{\,2} = \rho^2 \begin{bmatrix} \cos 2\varphi \\ \sin 2\varphi \end{bmatrix}$, Eq. (19) could be rewritten as

$$W_{\mathrm{AST}_3} = \begin{bmatrix} \frac{W_{222}(\vec{H}_x^2 - \vec{H}_y^2)}{2} - \vec{H}_x\vec{A}_{222,x} + \vec{H}_y\vec{A}_{222,y} + \frac{\vec{B}^2_{222,x}}{2} \\ W_{222}\vec{H}_x\vec{H}_y - \vec{H}_x\vec{A}_{222,y} - \vec{H}_y\vec{A}_{222,x} + \frac{\vec{B}^2_{222,y}}{2} \end{bmatrix} \cdot \begin{bmatrix} |\vec{\rho}|^2 \cos(2\varphi) \\ |\vec{\rho}|^2 \sin(2\varphi) \end{bmatrix}. \tag{20}$$

Then, according to the Zernike astigmatism coefficients (C_5 and C_6), we can obtain

$$\begin{bmatrix} -\vec{H}_x & \vec{H}_y & \frac{1}{2} & 0 \\ -\vec{H}_y & -\vec{H}_x & 0 & \frac{1}{2} \end{bmatrix} \begin{bmatrix} \vec{A}_{222,x} \\ \vec{A}_{222,y} \\ \vec{B}^2_{222,x} \\ \vec{B}^2_{222,y} \end{bmatrix} = \begin{bmatrix} C_5(\vec{H}) - \frac{W_{222}}{2}\left(\vec{H}_x^2 - \vec{H}_y^2\right) \\ C_6(\vec{H}) - W_{222}\vec{H}_x\vec{H}_y \end{bmatrix}. \quad (21)$$

Therefore, we can obtain

$$\begin{bmatrix} -\vec{H}_x & \vec{H}_y & \frac{1}{2} & 0 \\ -\vec{H}_y & -\vec{H}_x & 0 & \frac{1}{2} \end{bmatrix} \begin{bmatrix} \vec{\sigma}^{(\mathrm{sph})}_{\mathrm{PM},x} & \vec{\sigma}^{(\mathrm{asph})}_{\mathrm{PM},x} & \vec{\sigma}^{(\mathrm{sph})}_{\mathrm{SM},x} \\ \vec{\sigma}^{(\mathrm{sph})}_{\mathrm{PM},y} & \vec{\sigma}^{(\mathrm{asph})}_{\mathrm{PM},y} & \vec{\sigma}^{(\mathrm{sph})}_{\mathrm{SM},y} \\ \vec{\sigma}^{(\mathrm{sph})2}_{\mathrm{PM},x} - \vec{\sigma}^{(\mathrm{sph})2}_{\mathrm{PM},y} & \vec{\sigma}^{(\mathrm{asph})2}_{\mathrm{PM},x} - \vec{\sigma}^{(\mathrm{asph})2}_{\mathrm{PM},y} & \vec{\sigma}^{(\mathrm{sph})2}_{\mathrm{SM},x} - \vec{\sigma}^{(\mathrm{sph})2}_{\mathrm{SM},y} \\ 2\vec{\sigma}^{(\mathrm{sph})}_{\mathrm{PM},x}\vec{\sigma}^{(\mathrm{sph})}_{\mathrm{PM},y} & 2\vec{\sigma}^{(\mathrm{asph})}_{\mathrm{PM},x}\vec{\sigma}^{(\mathrm{asph})}_{\mathrm{PM},y} & 2\vec{\sigma}^{(\mathrm{sph})}_{\mathrm{SM},x}\vec{\sigma}^{(\mathrm{sph})}_{\mathrm{SM},y} \end{bmatrix} \begin{bmatrix} W^{\mathrm{sph}}_{222,\mathrm{PM}} \\ W^{\mathrm{asph}}_{222,\mathrm{PM}} \\ W^{\mathrm{sph}}_{222,\mathrm{SM}} \end{bmatrix} = \begin{bmatrix} C_5(\vec{H}) - \frac{W_{222}}{2}\left(\vec{H}_x^2 - \vec{H}_y^2\right) \\ C_6(\vec{H}) - W_{222}\vec{H}_x\vec{H}_y \end{bmatrix}. \quad (22)$$

Equation (22) gives the analytical expression between the field-center displacement vectors and the Zernike astigmatism coefficients.

E. Astigmatic Aberration Field Introduced by Astigmatic Figure Error of the PM

Due to the influence of gravity or support stress, the astigmatic figure error is easily generated on the large-aperture PM. For the astigmatic figure error on the nonstop surface, due to the different positions of the ray on the PM in different FOV, the contribution of the astigmatic figure error to the wave aberration is different in different FOV, as shown in Fig. 2.

In the FOV $\vec{H}$, the normalized decenter $\Delta\vec{h}$ of the imaging center relative to the aperture center of the PM is

$$\Delta\vec{h} = \bar{u}t\vec{H}/y, \quad (23)$$

where $\bar{u}$ is the slope angle of the chief ray of the maximum FOV on the PM, t is the distance between the entrance pupil and the PM, and y is the height of the pupil.

When the PM is with the astigmatic figure error, its wavefront contribution to the FOV $\vec{H}$ is

$$W(\vec{H},\vec{\rho}) = \Delta n \sum_n C_n \cdot Z_n\left[\pm(\vec{\rho} + \Delta\vec{h})\right]. \quad (24)$$

If there are an even number of intermediate images between the PM and the exit pupil, $(\vec{\rho}' + \Delta\vec{h})$ takes a positive sign; otherwise, $(\vec{\rho}' + \Delta\vec{h})$ takes a negative sign. Where Δn is the change of index in optical space before/after the surface, for the PM, Δn is -2. The contribution of the astigmatic figure error of the PM to the wavefront of the FOV $\vec{H}$ is

$$W(\vec{H},\vec{\rho}) = \Delta n \begin{bmatrix} C5 \\ C6 \end{bmatrix} \cdot (\vec{\rho} + \Delta\vec{h})^2 = \underbrace{\Delta n \begin{bmatrix} C5 \\ C6 \end{bmatrix} \cdot \vec{\rho}^2}_{\text{Astigmatism}} + \underbrace{\Delta n \begin{bmatrix} C5 \\ C6 \end{bmatrix} \cdot 2\Delta\vec{h}\vec{\rho}}_{\text{Tilt}} + \underbrace{\Delta n \begin{bmatrix} C5 \\ C6 \end{bmatrix} \cdot \Delta\vec{h}^2}_{\text{Piston}}. \quad (25)$$

As shown in Eq. (25), for the two-mirror telescopes with the stop on the SM, when there is astigmatic figure error on the PM, the off-axis FOV has more tilt and piston contributions than the on-axis FOV, but the astigmatic contribution is the same. Therefore, when there is an astigmatic figure error on the PM (represented by fringe Zernike coefficients C_5 and C_6), Eq. (25) should be rewritten as

$$\begin{bmatrix} -\vec{H}_x & \vec{H}_y & \frac{1}{2} & 0 \\ -\vec{H}_y & -\vec{H}_x & 0 & \frac{1}{2} \end{bmatrix} \begin{bmatrix} \vec{\sigma}^{(\mathrm{sph})}_{\mathrm{PM},x} & \vec{\sigma}^{(\mathrm{asph})}_{\mathrm{PM},x} & \vec{\sigma}^{(\mathrm{sph})}_{\mathrm{SM},x} \\ \vec{\sigma}^{(\mathrm{sph})}_{\mathrm{PM},y} & \vec{\sigma}^{(\mathrm{asph})}_{\mathrm{PM},y} & \vec{\sigma}^{(\mathrm{sph})}_{\mathrm{SM},y} \\ \vec{\sigma}^{(\mathrm{sph})2}_{\mathrm{PM},x} - \vec{\sigma}^{(\mathrm{sph})2}_{\mathrm{PM},y} & \vec{\sigma}^{(\mathrm{asph})2}_{\mathrm{PM},x} - \vec{\sigma}^{(\mathrm{asph})2}_{\mathrm{PM},y} & \vec{\sigma}^{(\mathrm{sph})2}_{\mathrm{SM},x} - \vec{\sigma}^{(\mathrm{sph})2}_{\mathrm{SM},y} \\ 2\vec{\sigma}^{(\mathrm{sph})}_{\mathrm{PM},x}\vec{\sigma}^{(\mathrm{sph})}_{\mathrm{PM},y} & 2\vec{\sigma}^{(\mathrm{asph})}_{\mathrm{PM},x}\vec{\sigma}^{(\mathrm{asph})}_{\mathrm{PM},y} & 2\vec{\sigma}^{(\mathrm{sph})}_{\mathrm{SM},x}\vec{\sigma}^{(\mathrm{sph})}_{\mathrm{SM},y} \end{bmatrix} \begin{bmatrix} W^{\mathrm{sph}}_{222,\mathrm{PM}} \\ W^{\mathrm{asph}}_{222,\mathrm{PM}} \\ W^{\mathrm{sph}}_{222,\mathrm{SM}} \end{bmatrix} = \begin{bmatrix} C_5 + 2_{(\mathrm{FIGURE})}C_5 - \frac{W_{222}\left(\vec{H}_x^2 - \vec{H}_y^2\right)}{2} \\ C_6 + 2_{(\mathrm{FIGURE})}C_6 - \vec{H}_x\vec{H}_y W_{222} \end{bmatrix}. \quad (26)$$

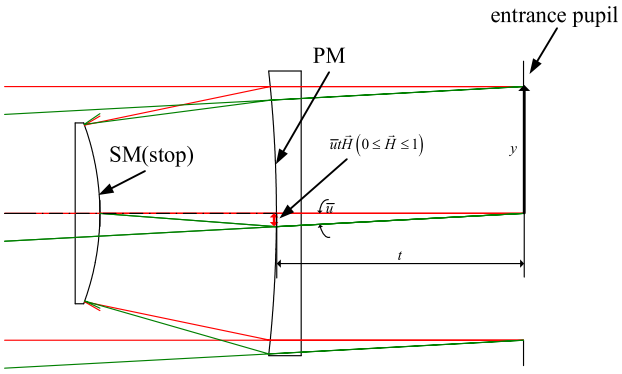

Fig. 2. Different FOV have different positions of the ray on the PM.

Per the analyzed model of the misalignments, the astigmatism figure error of the PM and the wavefront Zernike coefficients could be established by Eqs. (11–14), (18), (22), and (26).

3. SIMULATION EXPERIMENT

A. Model Prediction Accuracy for Misalignment Aberrations

In this section, an F/8 Cassegrain telescope will be used to verify the prediction accuracy of misalignment aberrations with our model. The aperture of the telescope is 1000 mm, and the FOV is ±0.5°. The Cassegrain telescope's optical parameters are shown in Table 1; its layout is shown in Fig. 3.

Table 1. Optical Parameters of the Cassegrain Telescope

Surface	Type	Conic	Radius of Curvature (mm)	Thickness (mm)
PM	Quadric	−1	−2666.667	−1000
SM (stop)	Quadric	−1.96	−800	2000
Image	–	–	−368.449	–

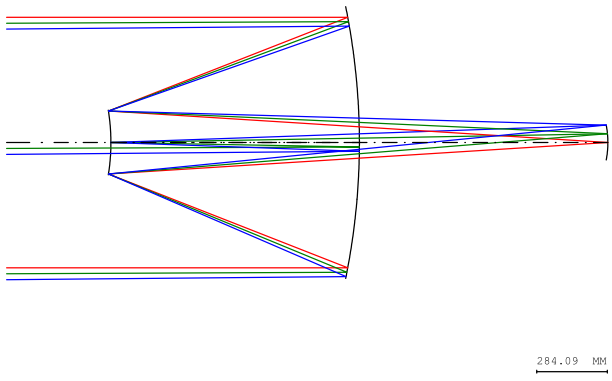

Fig. 3. Layout of Cassegrain telescope.

Table 2. Wave Aberration Coefficients of Cassegrain Telescope[a]

Surface	$W_{040}(\lambda)$	$W_{131}(\lambda)$	$W_{222}(\lambda)$	$W_{220M}(\lambda)$	$W_{311}(\lambda)$
PM (sph)	1302.109	−606.045	70.518	−5.641	−6.892
PM (asph)	−1302.109	363.627	−25.387	0.000	1.772
SM (sph)	−369.232	235.684	−37.610	18.805	0.000
SM (asph)	369.232	0.000	0.000	0.000	0.000
Sum	0.000	−6.734	7.522	13.163	−5.120

[a]λ = 632.8 nm, the same below.

The telescope's wave aberration coefficients can be calculated by the Seidel formula; the calculation results are shown in Table 2.

Using the FFD function of Code V, we can obtain the telescope's coma and astigmatism fields, as shown in Fig. 4. When the telescope is not misaligned, these two aberration fields are axisymmetric, and the coma and astigmatism are both zero at the center point of the FOV. The coma varies linearly with the FOV, and the average coma of the full FOV is 1.96λ. The astigmatism changes with the quadratic side of the FOV, and the average astigmatism of the full FOV is 3.06λ. The average wave aberration of the telescope is 1.40λ.

Table 3. Set of Random Misalignments

Type	XDE_{PM} (mm)	YDE_{PM} (mm)	ADE_{PM} (deg)	BDE_{PM} (deg)	C_{5-f} (λ)	C_{6-f} (λ)
Value	0.25	−0.2	−0.003	−0.005	1	−1.5

In order to verify the model in this paper, we randomly give a set of misalignments, as shown in Table 3.

Substituting the misalignments in Table 3 into the model of this paper, we can obtain the misaligned coma and astigmatism fields, which are predicted by the model in this paper, as shown in Fig. 5.

The binodal astigmatism in Fig. 5 is actually not strictly symmetrical about the central FOV. This is due to the influence of the misalignments, which introduces the astigmatism of the FOV asymmetry. Although the magnitude is small, it can also affect the symmetry of the dual nodes. The two astigmatism nodes in Fig. 5 are located at (−0.4°, 0.2°) FOV and (0.4°, −0.25°) FOV.

Using the FFD function of Code V, we can obtain the Zernike coma and astigmatism field map, as shown in Fig. 6.

The result of ray tracing can be used as the true value for comparison. The errors of Zernike coma and astigmatism predicted by the model in this paper relative to the ray tracing results are shown in Fig. 7.

The average errors of C_5, C_6, C_7, and C_8 are 0.040, 0.065, 0.057, and 0.058λ, respectively, and the corresponding average relative errors are 1.75%, 1.84%, 3.95%, and 4.10%, which confirms that the model in this paper has good accuracy.

B. Correction Effect of the Model for Misalignment Aberrations

The six misalignments in Table 3 could be calculated according to the Zernike coefficient. Since the testing results of one point

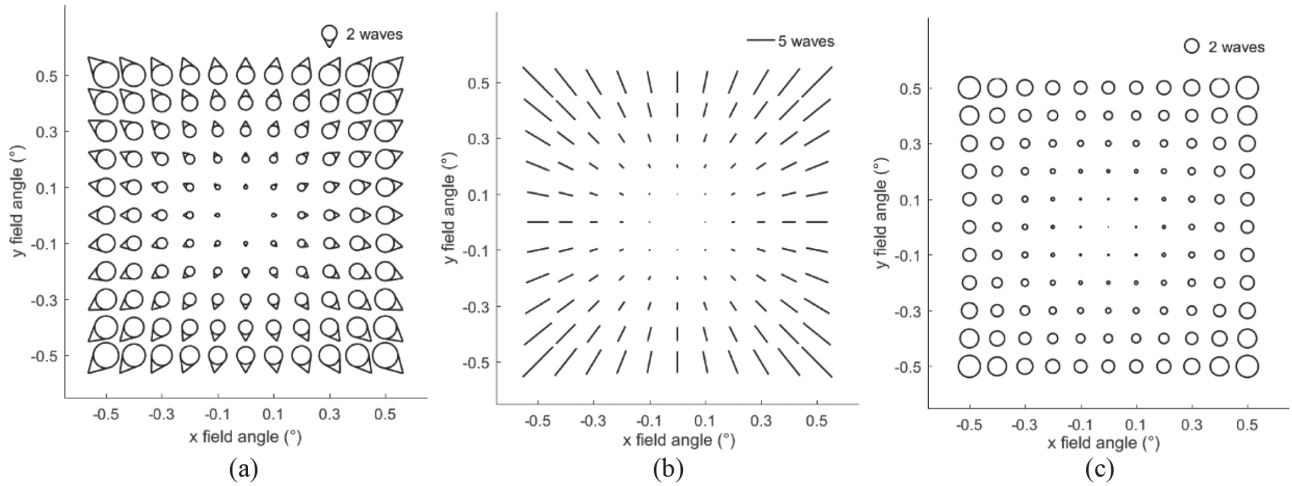

Fig. 4. When the telescope is not misaligned. (a) Coma field. (b) Astigmatism field. (c) Wave aberration RMS value.

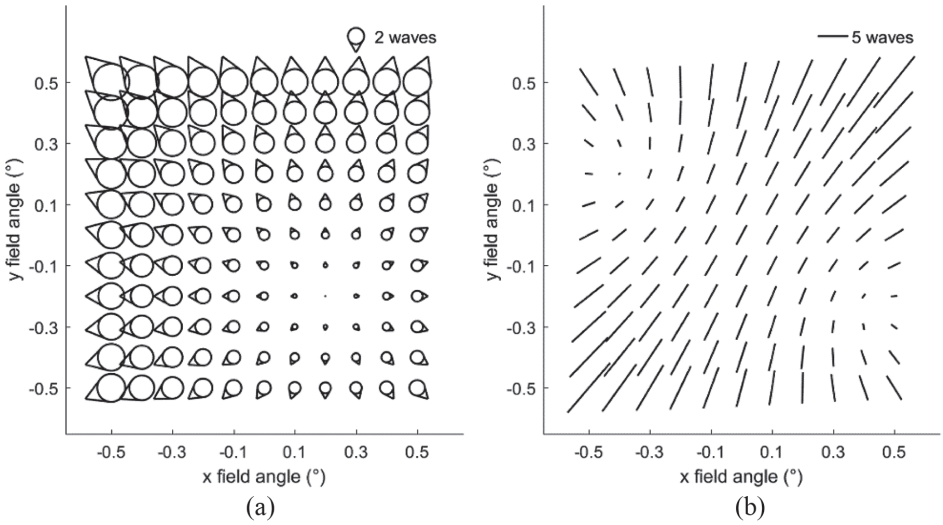

Fig. 5. When the system is misaligned, we predict (a) the coma field and (b) astigmatism field of the system by this model.

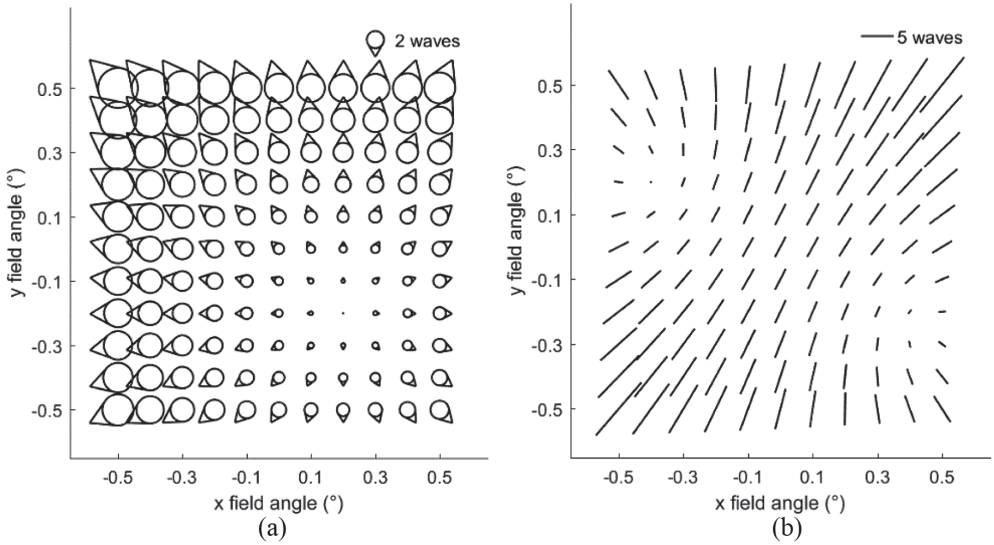

Fig. 6. When the system is misaligned. (a) Coma field and (b) astigmatism field of the system by ray tracing.

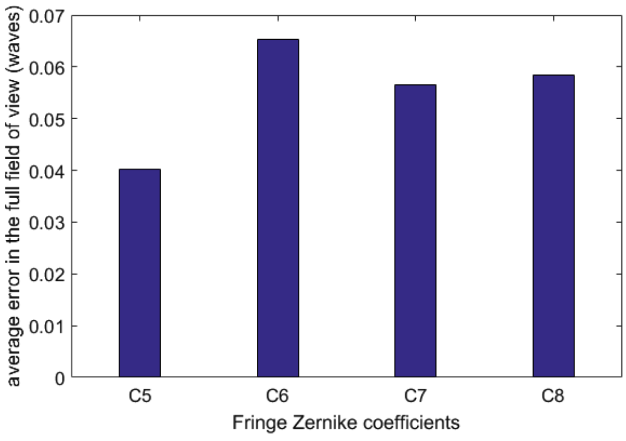

Fig. 7. Prediction error of misaligned fringe Zernike aberration coefficients C_5, C_6, C_7, and C_8.

Table 4. Zernike Aberration Coefficients for Two FOV Points by Ray Tracing

	C_5 (λ)	C_6 (λ)	C_7 (λ)	C_8 (λ)
(0°, 0°)	−1.950	2.927	0.886	−0.855
(0.5°, 0°)	−5.979	2.759	0.897	−3.211

of the FOV can list four equations, at least two FOV points need to be tested to solve the six misalignments. We select the wavefront Zernike coefficients of the central field point (0° and 0°) and the fringe field point (0.5° and 0°) for calculation. Using the wavefront analysis function of Code V, the Zernike coefficients of the above two FOV points could be obtained, as shown in Table 4.

Substituting the above Zernike coefficients into the model of this paper, six misalignments can be obtained, as shown in Table 5.

Table 5 also shows that the calculation errors of the decenter and the tilt misalignments are large, and the calculation accuracy

Table 5. Misalignments Calculated by the Model in This Paper

Type	XDE_{PM} (mm)	YDE_{PM} (mm)	ADE_{PM} (deg)	BDE_{PM} (deg)	$C_{5-f}(\lambda)$	$C_{6-f}(\lambda)$
Value	0.068817	−0.515662	−0.01716	0.00251	0.972905	−1.46421
Absolute error	−0.18118	−0.31566	−0.01416	0.00751	−0.0271	0.03579
Relative error	72.47%	157.83%	472.00%	150.20%	2.71%	2.39%

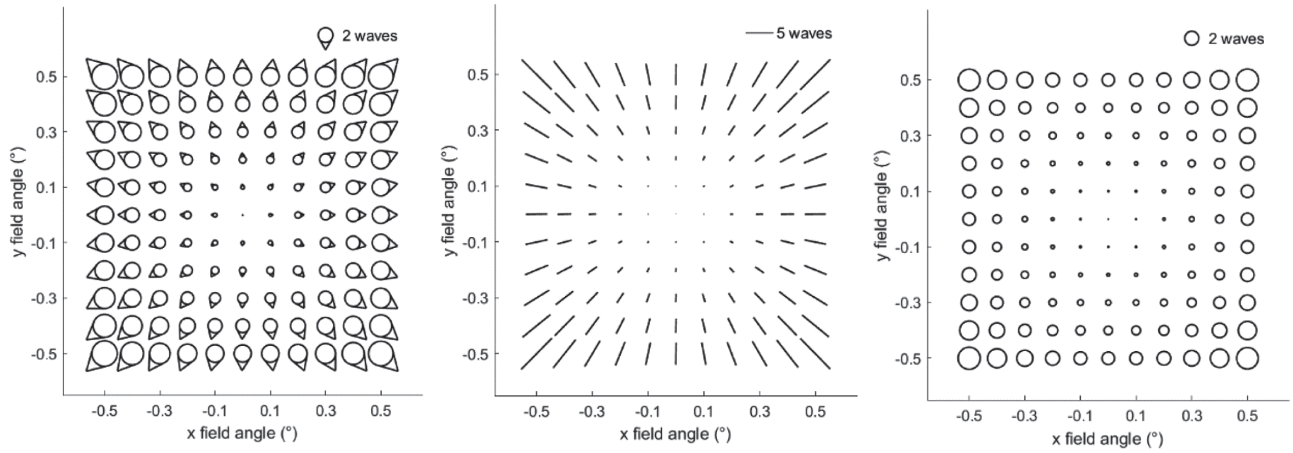

(a) (b) (c)

Fig. 8. FFDs for fringe Zernike coefficients after system correction based on calculated misalignments. (a) $C_{7/8}$, (b) $C_{5/6}$, and (c) RMS wavefront error for the nominal Cassegrain telescope.

Table 6. Misalignments Calculated by the Model with Boresight Error Added in This Paper

Type	XDE_{PM} (mm)	YDE_{PM} (mm)	ADE_{PM} (deg)	BDE_{PM} (deg)	$C_{5-f}(\lambda)$	$C_{6-f}(\lambda)$
Value	0.22754	−0.19214	−0.00283	−0.00452	0.97023	−1.47272
Absolute error	0.02246	−0.00786	−0.00017	−0.00048	0.02977	−0.02728
Relative error	8.99%	3.93%	5.63%	9.65%	2.98%	1.82%

of the astigmatic figure error is high. The wave aberration field obtained after correcting the misaligned system according to the calculated misalignments is shown in Fig. 8.

After correction, the average coma and astigmatism in the FOV are 1.96 and 3.06 λ, respectively, which show that it is consistent with the designed state in distribution and magnitude. It can be seen that the aberrations caused by decentering and tilt compensate each other, resulting in a relatively large calculation error of decentering and tilt; thus, even if the decentering and tilt of the system do not reach the designed values, the system still has the same image quality as the design state. That is to say, the PM not only has good image quality in the design state but also can achieve the design image quality because of the aberration compensation in a certain misalignment state. However, since the astigmatic figure error cannot be compensated by other degrees of freedom, the calculation accuracy is high and basically returns to the design state. In general, because the telescope's user pays more attention to the imaging quality of the system rather than whether the decentering and tilt of the system can be restored to the designed state, the method in this paper is effective from the perspective of aberration correction.

At the same time, we found that, if we can detect the boresight error and add the analytical relationship between boresight error and misalignments in the model, the solution accuracy of the misalignments could be greatly improved. By tracing the OAR rays, the calculation formula of the boresight error $\Delta\vec{H}_{IMG}$ can be obtained:

$$\Delta\vec{H}_{IMG} = \begin{bmatrix} \frac{2d_2(XDE_{PM} - BDE_{PM} r_{PM})}{2d_1 - r_{PM}} \\ \frac{2d_2(YDE_{PM} + ADE_{PM} r_{PM})}{2d_1 - r_{PM}} \end{bmatrix}. \quad (27)$$

A new model is established from Eqs. (11–14), (18), (26), and (27); the calculated misalignments are shown in Table 6.

According to the solution result in Table 6, we correct the misaligned system. The wave aberration field and the RMS value of the wave aberration are shown in Fig. 9.

As also shown in Fig. 9, the image quality is restored to the design state after adding the boresight error for correction, and the solution accuracy of the misalignments is greatly improved.

4. CONCLUSION

In this paper, for the two-mirror telescopes with stop on the SM, the NAT theory is used to analyze the quantitative analytic expression among the misalignment aberration, the astigmatism figure error of the PM, and the misalignments, and a correction model for the system misalignment aberration is established. We use a Cassegrain telescope as an example to verify the prediction accuracy of the model for misalignment aberration. The results show that the prediction accuracy of the misalignment coma and astigmatism based on this model is high, and the

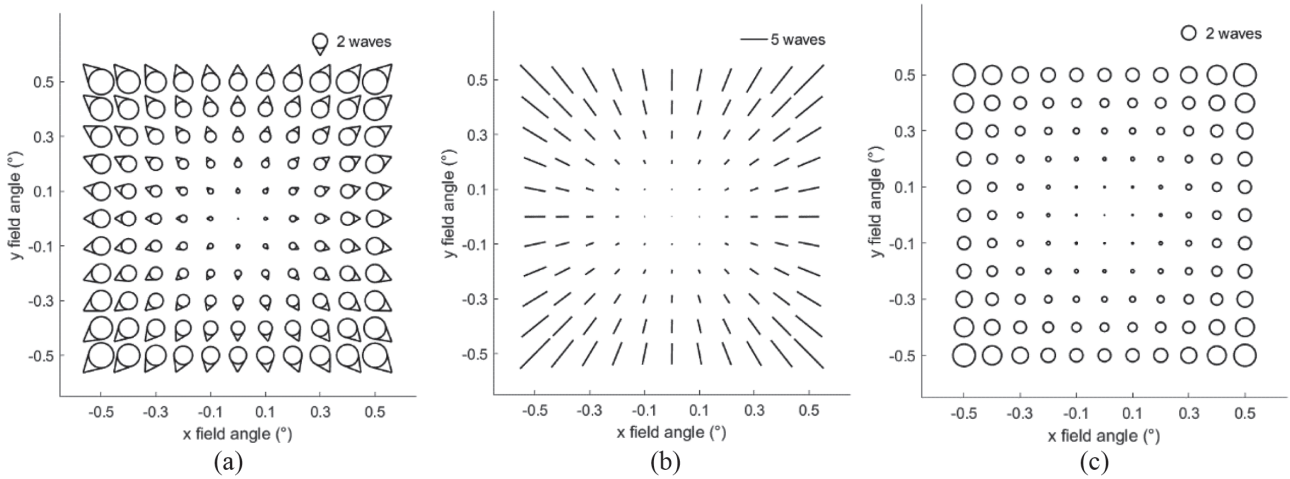

Fig. 9. FFDs for fringe Zernike coefficients after system correction based on calculated misalignments after adding the detection of boresight error. (a) $C_{7/8}$, (b) $C_{5/6}$, and (c) nominal RMS wavefront error for the telescope.

relative error of prediction is less than 4.1%. The aberration correction of the misaligned system is carried out through the misalignment aberration correction model in this paper. The misalignment calculation and the actual value are quite different, but the aberration correction result is consistent with the design state. After adding the boresight error in the model, the calculation error of the misalignments could be reduced to less than 10%, and the aberration correction result is also consistent with the design state.

Funding. National Science Fund for Distinguished Young Scholars (62105331).

Disclosures. The authors declare no conflicts of interest.

Data availability. Data underlying the results presented in this paper are not publicly available at this time but may be obtained from the authors upon reasonable request.

REFERENCES

1. T. Schmid, K. P. Thompson, and J. P. Rolland, "Misalignment-induced nodal aberration fields in two-mirror astronomical telescopes," Appl. Opt. **49**, D131–D144 (2010).
2. T. Schmid, K. P. Thompson, and J. P. Rolland, "A unique astigmatic nodal property in misaligned Ritchey-Chrétien telescopes with misalignment coma removed," Opt. Express **18**, 5282–5288 (2010).
3. T. Schmid, J. P. Rolland, A. Rakich, and K. P. Thompson, "Separation of the effects of astigmatic figure error from misalignments using nodal aberration theory (NAT)," Opt. Express **18**, 17433–17447 (2010).
4. Z. Gu, Y. Wang, G. Ju, and C. Yan, "Computation of misalignment and primary mirror astigmatism figure error of two-mirror telescopes," J. Astron. Telesc. Inst. **4**, 019002 (2018).
5. G. Ju, C. Yan, Z. Gu, and H. Ma, "Computation of astigmatic and trefoil figure errors and misalignments for two-mirror telescopes using nodal-aberration theory," Appl. Opt. **55**, 3373–3386 (2016).
6. M. Liang, V. Krabbendam, C. F. Claver, S. Chandrasekharan, and B. Xin, "Active optics in large synoptic survey telescope," Proc. SPIE **8444**, 84444Q (2012).
7. R. Upton and T. Rimmele, "Active reconstruction and alignment strategies for the advanced technology solar telescope," Proc. SPIE **7793**, 77930E (2010).
8. S. Kim, H.-S. Yang, Y.-W. Lee, and S.-W. Kim, "Merit function regression method for efficient alignment control of two-mirror optical systems," Opt. Express **15**, 5059–5068 (2007).
9. W. Wu, J. Shang, Z. Luo, D. Fang, and Z. Deng, "Misalignments computation of a two-mirror optical system based on modified merit function regression method," IOP Conf. Ser. Mater. Sci. Eng. **677**, 032063 (2019).
10. D. Gallieni, C. Del Vecchio, E. Anaclerio, and P. G. Lazzarini, "LBT adaptive secondary preliminary design," Proc. SPIE **4007**, 508–515 (2000).
11. K. P. Thompson, T. Schmid, O. Cakmakci, and J. P. Rolland, "Real-ray-based method for locating individual surface aberration field centers in imaging optical systems without rotational symmetry," J. Opt. Soc. Am. A **26**, 1503–1517 (2009).
12. K. P. Thompson, "Aberration fields in tilted and decentered optical systems, " Ph.D. dissertation (University of Arizona, 1980).